Non-invasive ultrasonic surgery of the brain in non-human primates

Fabrice Marquet
Institut Langevin, ESPCI-ParisTech, CNRS UMR7587, INSERM U979, Paris, France

Anne-Laure Boch
Department of Neurosurgery, Groupe Hospitalier Pitié-Salpêtrière, Paris, France

Mathieu Pernot and Gabriel Montaldo
Institut Langevin, ESPCI-ParisTech, CNRS UMR7587, INSERM U979, Paris, France

Danielle Seilhean
Department of Neuropathology, Groupe Hospitalier Pitié-Salpêtrière, AP-HP, UPMC, CRICM Inserm UMR_S975/CNRS UMR7225, Paris, France

Mathias Fink, Mickael Tanter, and Jean-Francois Aubry[a)]
Institut Langevin, ESPCI-ParisTech, CNRS UMR7587, INSERM U979, Paris, France

(Received 30 September 2012; revised 2 April 2013; accepted 8 April 2013)

High-intensity focused ultrasound causes selective tissue necrosis efficiently and safely, namely, in the prostate, liver, and uterine fibroid. Nevertheless, ablation of brain tissue using focused ultrasound remains limited due to strong aberrations induced by the skull. To achieve ultrasonic transcranial brain ablation, such aberrations have to be compensated. In this study, non-invasive therapy was performed on monkeys using adaptive correction of the therapeutic beam and 3D simulations of transcranial wave propagation based on 3D computed tomographic (CT) scan information. The aim of the study was two-fold: induce lesions in a non-human primate brain non-invasively and investigate the potential side effects. Stereotactic targeting was performed on five *Macaca fascicularis* individuals. Each hemisphere was treated separately with a 15-day interval and animals were sacrificed two days after the last treatment. The ultrasonic dose delivered at the focus was increased from one treatment location to the other to estimate the thermal dose for tissue alteration. Thermal doses in the brain were determined by numerical computations. Treatment efficiency and safety were evaluated histologically. The threshold for tissue damage in the brain was measured to be between 90 and 280 cumulative equivalent minutes at 43 °C. Intravenous injection of corticoids before the treatment limited the side effects.
 [http://dx.doi.org/10.1121/1.4812888]

PACS number(s): 43.80.Sh, 43.60.Tj [ROC] Pages: 1632–1639

I. INTRODUCTION

In the 1920s, a few years after Paul Langevin paved the way for generating high-intensity ultrasound while developing the sound navigation and ranging (SONAR) (Chilowsky and Langevin, 1916), the biological effects of ultrasound were investigated and potential medical applications highlighted (Harvey and Loomis, 1928; Wood and Loomis, 1927). The ability of focused ultrasound to ablate tissue rapidly raised new hopes to target the brain non-invasively. Lynn *et al*. (1942) pioneered the targeting of neurological symptoms in dogs by transcranially applying focused ultrasound at a frequency of 835 kHz. However, as stated by Lynn *et al*. (1942), "unfortunately, there was always a necrosis of the scalp where the apparatus was applied." In 1949, Lars Leksell commercialized the first stereotactic frame, allowing precise positioning of surgical tools, including ultrasonic transducers. As ultrasonic focusing was hampered by the skull, a craniectomy was performed in front of the transducer. Lindstrom (1954) used Leksell's ultrasonic device to perform prefrontal ultrasonic transdural ablation, presenting it as a substitute for lobotomy. Lars Leksell successfully bypassed the ultrasonic aberration of the skull by switching from ultrasound to radiotherapy. This technique has been progressively improved (Andrews *et al*., 2006; Chang and Adler, 2001) and is still the safest and most efficient technique for non-invasive ablation of brain tissue in clinical practice. At the same time as Leksell's investigations on ultrasound, William and Francis Fry developed their own prototype and proved the ability to produce discrete deep lesions in the brain (Fry *et al*., 1954; Fry *et al*., 1955; Fry, 1956), by performing a craniotomy prior to the treatment and establishing quantitative thresholds for inducing permanent changes in brain tissues (Fry *et al*., 1970). Francis Fry further investigated the possibility of focusing through the skull by decreasing the frequency to 500 kHz. Nevertheless, even though focusing was possible, the foci tended to be distorted and shifted (Fry and Goss, 1980).

In the 1990s, time-reversal-based techniques (Thomas and Fink, 1996) or phase conjugation (Hynynen and Jolesz, 1998) were introduced to correct the aberrations induced by

[a)]Author to whom correspondence should be addressed. Electronic mail: jean-francois.aubry@espci.fr

the skull bone. Based on time reversal, a sharp focus was restored through the skull of living large animals (sheep; Pernot *et al*., 2007), to achieve thermal coagulation of brain tissues. This study was limited by the use of a minimally invasive technique. It required implanting temporarily a hydrophone inside the brain before the treatment to correct the aberration (Pernot *et al*., 2007). This limitation, however, can be overcome. The possibility to deduce the acoustical properties of the skull from magnetic resonance imaging (MRI) (Sun and Hynynen, 1998) or computed tomography (CT) (Aubry *et al*., 2003) raised new hopes for non-invasive brain therapy. Propagation through the skull can thus be simulated with a 3D finite-difference code (Aubry *et al*., 2003), ray tracing (Sun and Hynynen, 1998), or hybrid approaches (Pulkkinen *et al*., 2011; Pinton *et al*., 2012). Once the distortions induced by the skull are predicted by simulation, they can be corrected by time reversal or phase conjugation. Recently, two clinical trials were performed with the brain version of the Exablate system (Insightec, Haifa, Israel) on neuropathic pain (Martin *et al*., 2009) and glioblastoma multiforme (GBM) (McDannold *et al*., 2010), respectively. McDannold *et al*. (2010) used the Exablate 3000 system and demonstrated its ability to target GBM, as well as locate the sonication site with magnetic resonance temperature imaging. The lack of power of the prototype prevented them from inducing a thermal necrosis, but extrapolation of the low sonication results proved that it is possible to ablate tissues in deep seated areas of the brain without overheating the skull vault. To increase the transmitted power, the same team proposed a switch to a lower frequency (220 kHz), given that low frequencies penetrate the skull bone more easily (Fry and Goss, 1980). Unfortunately, the first patient treated therapeutically at 220 KHz died five days after treatment from serious hemorrhaging (Jolesz, 2008). A more powerful version of the 660-kHz prototype (Exablate 4000 system, Insightec) has been developed (Monteith *et al*., 2013a). Elias *et al*. at the University of Virginia have begun an FDA-approved phase 1 trial on the treatment of essential tremor using this prototype (Monteith *et al*., 2013b). Moreover, Martin *et al*. (2009) in Zurich treated nine patients with chronic neuropathic pain, and observed no side effects or neurological deficits and a moderate heating in the brain (up to 60 °C). Unfortunately, in the follow-up study including more patients, Martin *et al*. (2009) reported a complication during post-treatment MRI: a bleed at the target site, with ischemia in the motor thalamus (Jeanmonod *et al*., 2012). The bleeding at the focus did not produce deficits, but the ischemia (out of focus) induced a typical motor symptomatology. The adverse events reported in these two clinical tests highlight the importance of *in vivo* studies on transcranial focused ultrasound, as well as histological data, to support safe clinical translation. Such studies need to be performed in an animal model with a head shape similar to that of a human. Non-human primates are therefore a suitable model to investigate the clinical potential of this technique. McDannold *et al*. (2003) reported non-invasive *in vivo* thermal lesions obtained in trepanned monkeys. The same team extended this approach by performing magnetic resonance (MR)-guided sonications through the intact skull in monkeys. As mentioned in the paper (Hynynen, 2006), "these experiments were designed to establish the maximum intensity levels that could be delivered through the living skull bone" and no lesions in the targeted brain tissues were reported: "it was not possible to induce brain tissue coagulation at the focus without overheating the brain surface".

The purpose of this study was to induce brain tissue coagulation in the brain of monkeys and investigate the remote effects, using an intact skull to take into account the potential effect of a closed brain cavity. This was achieved using a high-frequency system (1 MHz) with a tight focus that optimized the antenna gain. CT guidance was used to target the brain tissues as the system was applied in an animal facility without MR. Thermal doses in the brain were therefore estimated from numerical computations and not from MR temperature monitoring.

II. MATERIAL AND METHODS

A. High power prototype

Three hundred high-power piezocomposite transducers (8 mm diameter, 0.5 cm^2 active area, 1 MHz central frequency, Imasonic, Besançon, France) were mounted semi-randomly onto a spherical surface [Fig. 1(a)] with a 14-cm

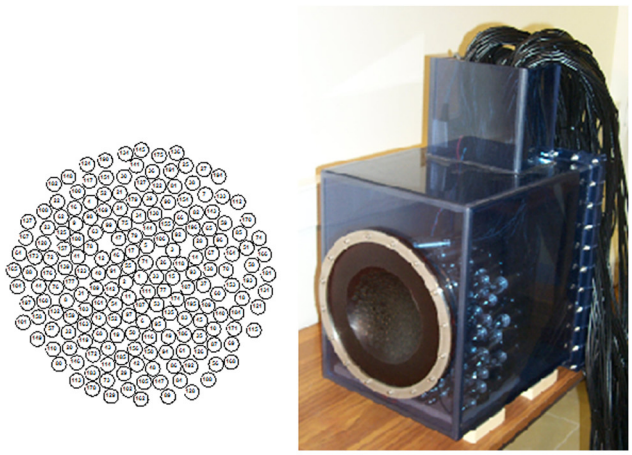

(a)

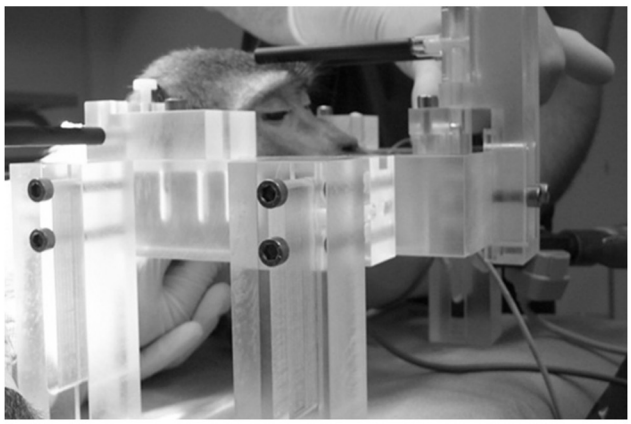

(b)

FIG. 1. (Color online) (a) General view of the therapeutic array (right) and a diagram of the arrangement of the 300 elements (left). (b) Stereotactic frame. The monkey's position is locked by four rods: two in the mouth and two in the ears.

radius of curvature and an aperture size of 20 cm (F number is 0.7). The transducers were connected to a 300-channel electronic driving system. Each electronic channel was individually programmable (phase and amplitude) and possessed its own emission/reception electronic board. Either continuous waves or pulsed programmable signals could be transmitted. A latex membrane filled with degassed water was fixed in front of the transducers. A pump circulated water through a chiller to cool it down to 14 °C. A thin layer of acoustic gel was applied to the skin and to the latex membrane before placing them in contact, to facilitate acoustical coupling.

B. Animal model

Although this prototype geometry was designed for non-invasive transcranial human brain treatment, it was first tested on five monkeys. This animal model was chosen because the size of its brain was sufficient and the stereotactic positioning could be performed with millimetric accuracy. At this stage, no tumor was implanted in the animal's brain as the aim was to check if it was possible to concentrate enough energy through the skull to induce thermal lesions in deep-seated tissues (2 cm deep in this study). Experiments were conducted in a sterile environment. Each monkey was tranquillized with Hypnovel® (midazolam, 0.5 mg/kg,IV) and then deeply anesthetized with Penthotal® (Thiopental, 10 mg/kg,IV). The animal's rectal temperature was monitored with a thermocouple. Hairs on the animal's head were removed with hair clippers and depilatory cream.

C. Stereotactic positioning

To ensure millimetric positioning, a stereotactic frame was built in house. Its design was derived from the stereotactic frames used in cranial surgery for large animals (cats, dogs, and monkeys). The position of the monkey head with respect to the frame was locked by two rods in the mouth and two rods in the ears of the animal. Figure 1(b) shows an image of this positioning. Seven days before treatment, the animal was anesthetized and a CT scan performed with the frame mounted on the head. The ear rods mechanically locked the antero-posterior and superior−inferior positions. Therefore, the error in the repositioning process was mainly lateral. Graduations along the rods allowed a reposition error of 0.5 mm. Rotation of the head was blocked by the mouth rods. The position of the mouth rods was kept unchanged during repositioning. Immediately after the scan, the stereotactic frame was removed and the treatment planning performed.

D. Treatment planning

Using 3D CT scan data, the whole volume of the monkey skull was reconstructed so that the neurosurgeon could choose the target point (Fig. 2). By applying the electronic steering capabilities of the ultrasonic array, the target could be chosen at any location inside a 1.5-cm radius sphere centered on the geometrical focus. Targets were chosen at the center of the hemispheres, 2 cm from the outer surface of the brain, 2 cm away from the skull base, and 1 cm from the brain midline (Fig. 2).

The propagation of the ultrasonic wave from the target point to the array was then simulated by a 3D finite-difference simulation code developed at the Institut Langevin (Marquet *et al.*, 2009). Figure 3 shows an example of the propagation of a pulse through the monkey skull.

E. Treatment

The simulated wavefront was then time reversed (Tanter *et al.*, 2007), to compensate for diffraction and refraction effects induced by the skull bone, and finally convolved by a 10-s therapeutic wave (1 MHz) to generate a set of emission signals to be used for treatment. In practice, each transducer was driven by an independent electronic channel capable of generating a temporally inverted signal stored in memory.

For each targeted area, the treatment was as follows: a 10-s sonication at a fixed power was repeated 10 times at the same location with a 20-s cooling delay between sonications to allow the skin temperature to return to baseline. A mean temperature of 20 °C was measured in real time on the skin with a thermocouple (Iron-constantan, 40 μm diameter, PhysiTemp Corporation). The water-cooling system was

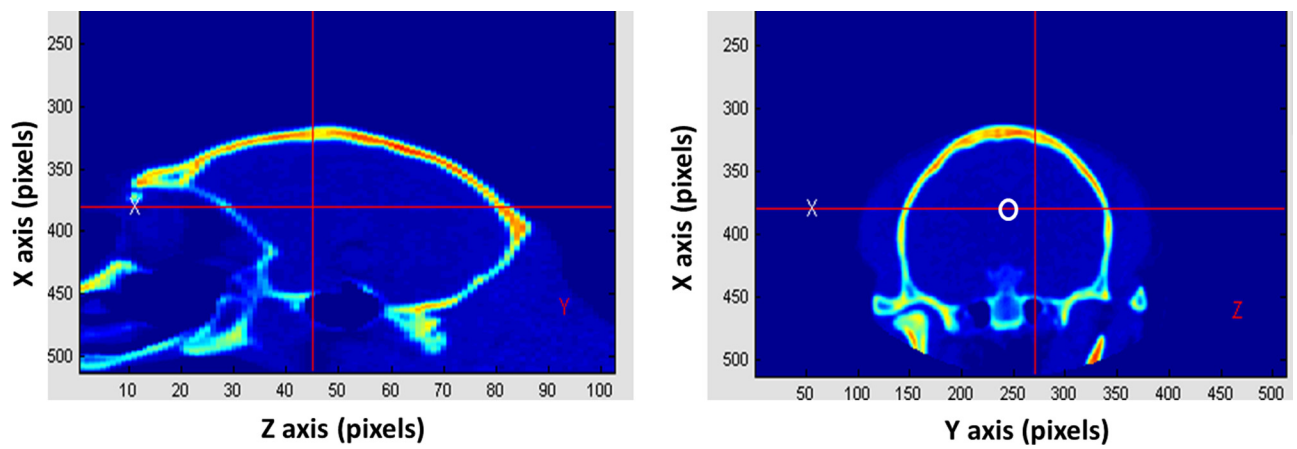

FIG. 2. (Color online) Example of sagittal and coronal CT slices showing the targeted point. In this case, the chosen target was located 1 cm away from the geometrical focus of the array (white circle in the center of the brain, right image). Treatment was performed by electronically steering the beam towards the target location.

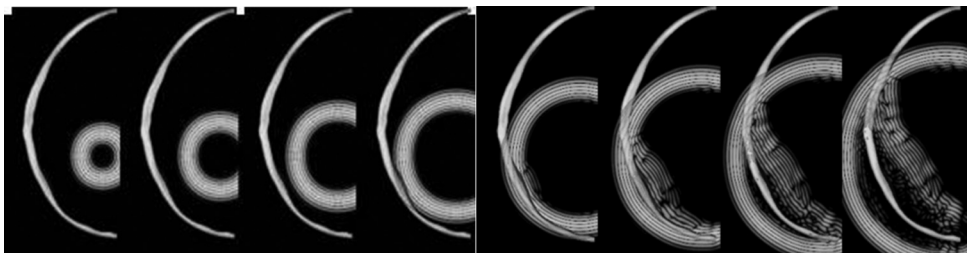

FIG. 3. 3D simulation of the ultrasonic propagation from the virtual source towards the therapeutic array through the skull bone using the 3D finite-difference scheme. Pressure field is displayed at a dB scale.

switched on during the entire treatment with the temperature set to 14 °C. The acoustic power was modified from one treatment location to another to explore various thermal depositions at the focus. The output power of the prototype ranged from 430 to 780 acoustical watts for the different experiments. It corresponded to pressure levels ranging from 7.5 to 15 MPa in water, as measured in a water tank with a calibrated hydrophone (HCN-0400, Onda Corporation, Sunnyvale, CA) mounted on step motors. Such measurements were conducted with the same electronic steering used during the treatment. The corresponding *in situ* pressure levels in the monkey brain were estimated numerically, taking into account the steering and the attenuation of soft tissue (skin muscle and brain) and the monkey skull attenuation. Monkey skull attenuation was measured retrospectively through extracted monkey skulls. *In situ* pressure ranged from 1.5 to 3 MPa. Each animal was first treated in the left hemisphere, woken up, and then followed up for 15 days. The procedure was repeated in the right hemisphere 15 days later. After the second treatment, the monkeys were kept under observation for two days before sacrifice. Immediately after sacrifice, the brain was extracted and immersed in a 4% formaldehyde solution. One hour after sacrifice, MR imaging of the explanted brain was performed (Sec. II F). Histology was performed four months later once the brain was completely fixed (Sec. II G). Figure 4 shows the animal being ready for treatment. Accurate positioning was ensured by the stereotactic frame.

Animal preparation and treatment planning were approved by the ethical committee of the IMM Research group.

F. Histology

The animals were sacrificed with pentobarbital. The whole brain was removed and fixed in 4% formaldehyde for four months. During macroscopic examination, brains were first cut into 5-mm-thick coronal slices. Twelve 1 cm × 1 cm tissue samples were selected. Based on treatment planning, the slice corresponding to the target was determined for each hemisphere and four samples were selected: one at the expected location of the target; one in contact with the skull vault; one in contact with the skull base; and one outside the focus but not peripheral (not in contact with the skull) in the remaining parts of the slice. Finally, four tissue samples were selected in other slices, including one in contact with the skull vault and one in contact with the skull base. Tissue samples were then numbered, but unlabeled for blinded

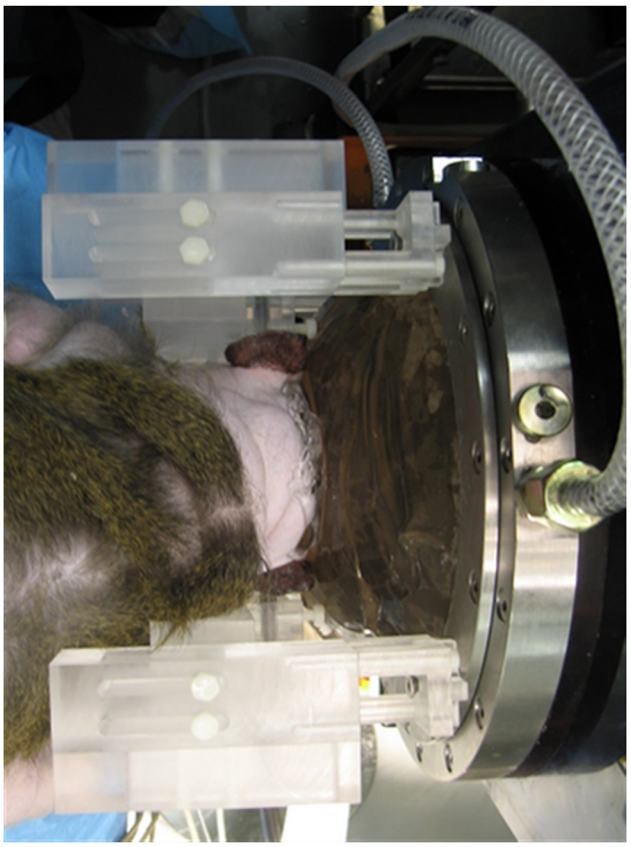

(a)

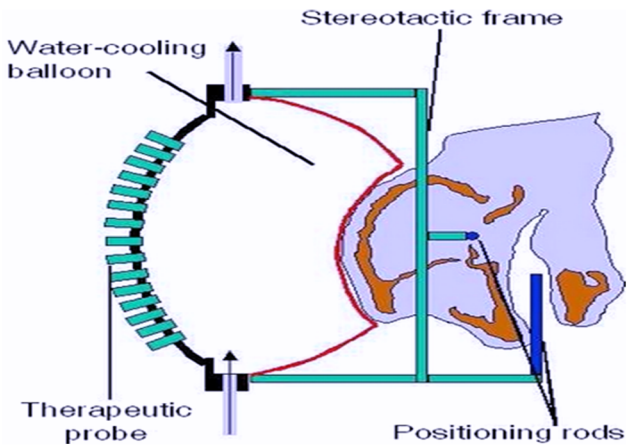

(b)

FIG. 4. (Color online) A photographic image (a) and schematic view (b) of treatment in one monkey. The monkey was placed in the stereotactic frame, which was fixed to the front part of the prototype.

histological examination. After paraffin embedding, 5-μm-thick sections were stained using hematoxylin and eosin, Masson's trichrome, and Periodic Acid Schiff (PAS) reagent.

G. Imaging modalities

Post-treatment images were taken on explanted and fixed brains with a 7 T MRI unit (Brucker), as can be seen in Fig. 5. Steady-state free precession images were acquired (TE = 1.35 ms, TR = 2.70 ms, flip angle = 30°, matrix = 128 × 128 × 128).

H. Estimated thermal dose

The thermal dose at the focus was estimated by numerical computation of the Penne's (1948) bioheat equation

$$\rho C_t \frac{\partial T}{\partial t} = \nabla \cdot k \nabla T + Q - W_b C_b (T - T_b),$$

where k is the thermal conductivity of the brain ($0.52\,\mathrm{W\,m^{-1}\,K^{-1}}$), C_t the thermal capacity of the brain ($3700\,\mathrm{J\,kg^{-1}\,K^{-1}}$), ρ the volumic mass of the brain, W_b the blood perfusion rate ($0.008\,\mathrm{s^{-1}}$), C_b the thermal capacity of the blood ($3700\,\mathrm{J\,kg^{-1}\,K^{-1}}$), and Q the acoustical energy deposited in the brain

$$Q = \frac{\alpha |p|^2}{\rho c},$$

where α is the absorption coefficient of the brain ($6\,\mathrm{Np.m^{-1}}$ at 1 MHz), c is the speed of sound ($1500\,\mathrm{m\,s^{-1}}$) and p the pressure amplitude in the brain.

The propagation through the skull of the therapeutic wave emitted by the array front was simulated using the same simulation tool applied for the planning. This estimated pressure distribution p was introduced into the bioheat equation to compute the temperature elevation in the brain as a function of time. This temperature enabled us to calculate the thermal dose (CEM 43 °C) at the focus according to the definition given by Sapareto and Dewey (1984)

$$\mathrm{CEM}\,43\,^{\circ}\mathrm{C} = \int_0^{t_T} R^{(43-T(t))} dt,$$

where t_T is the total treatment time in minutes, T is the temperature at time t, and R is a constant. R equals 0.25 if $T < 43\,^{\circ}\mathrm{C}$ and 0.5 if $T > 43\,^{\circ}\mathrm{C}$. By definition, the thermal dose corresponds to the cumulative number of equivalent minutes at 43 °C. The average thermal dose over the beam spot (−6 dB volume) was estimated for each experiment.

III. RESULTS

Tissues lesions were confirmed by histology in four or the eight sonications tested. They were characterized as ill-defined areas of acidophilic necrosis. These lesions were 1 to 3 mm large and deprived of inflammatory infiltrates. Figure 6 (PAS staining) shows an example of fibrinoid necrosis of a vessel wall surrounded by a ring of macrophages, similar to lesions that can be induced by radiotherapy. No lesion was found on the control samples. The histology results for the targeted locations were plotted as a function of the calculated thermal dose (Fig. 7). A sigmoid fit was made and superimposed onto the data points (solid line on Fig. 7). Due to the logarithmic scale, the sigmoid fit appeared as a straight line. A lesion was found on four out of the five targeted locations for thermal doses higher than 280 cumulative equivalent minutes (Eq min) at 43 °C. No lesions were observed for thermal doses lower than 90 Eq min at 43 °C. The 50% probability of necrosis given by the sigmoid fit corresponded to 192 Eq min at 43 °C.

One animal unfortunately could not tolerate the anesthesia and died during CT scanning; therefore, no treatment could be performed on this animal. The first monkey had a minor subcutaneous edema that resorbed rapidly.

The cooling time between sonications was sufficient to avoid skin burns in seven experiments. Interestingly, the only skin burn (on the second monkey) that was observed was not located exactly along the beam path, but rather at the rear of the head, at the boundary of the contact between the water balloon and the skin. Most probably an air bubble was trapped at this location, inducing strong overheating. This monkey also developed brain edemas and was consequently administered corticoids: Solumedrol was injected before treatment (30 mL/kg, slow intravenous injection) and Dexafort one day after treatment (0.05 mL/kg, intramuscular injection).

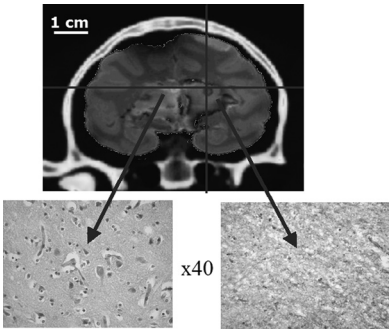

FIG. 5. Thermal lesion induced in the brain. Top: fusion of pretreatment CT and post-treatment MR images with the targeted point (at the center of the cross). Bottom: neuropathology (Masson's trichrome stain × 400); acidophilic necrosis (right) compared with normal tissues (left).

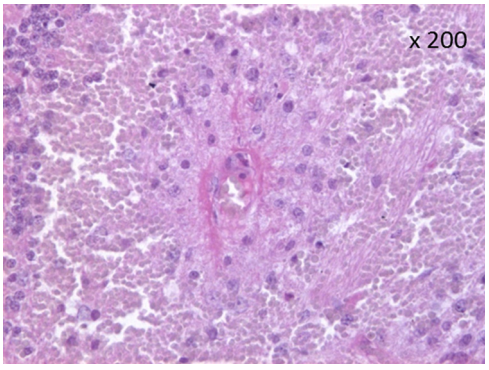

FIG. 6. (Color online) Fibrinoid necrosis of vessel wall (PAS stain × 200).

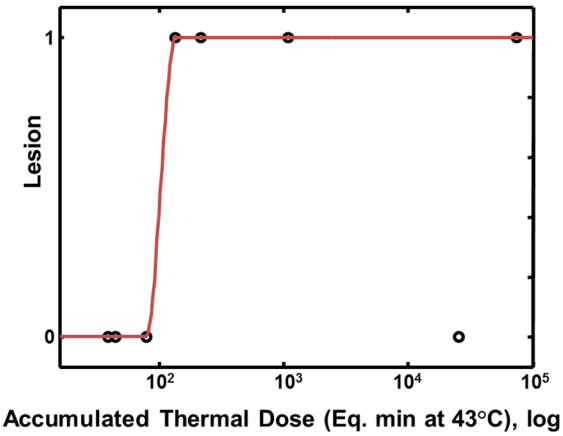

FIG. 7. (Color online) Tissue lesions observed during histological examination as a function of the thermal dose at the targeted location.

The third monkey presented no sign of side effects. The fourth one had a minor edema between the skin and skull bone above the eyes.

Animals were woken up after each treatment. A basic neurological examination was performed and the animals had a normal score after treatment. They were eating, moving, hearing and seeing normally, except monkey no. 2, which was listless and ate less. For all animals, except monkey no. 2, no significant alteration of brain function was noted during the follow-up period (17 days after the first treatment and 2 days after the second treatment). The results are summarized in Table I.

IV. DISCUSSION

A. Open skull/closed skull

Focused ultrasound ablation has already been achieved in the past in large animal brain tissues. However, in all cases, animals have a complete craniotomy to provide an acoustic window. In the 1950s, William and Francis Fry took advantage of a complete craniotomy to successfully produce discrete deep lesions in the brain (Fry *et al.*, 1954, 1955, 1970). Such a treatment was guided by ultrasonic monitoring. Nevertheless, due to the poor resolution and contrast of ultrasonic scanners available at that time, guidance and monitoring were poor. More recently, two groups proposed to use MR monitoring and developed MR-compatible therapeutic arrays. Due to craniectomy being performed prior to the treatment, such systems could induce lesions in the brain of 10 female pigs (Cohen *et al.*, 2007) and two male rhesus monkeys (McDannold *et al.*, 2003). These studies demonstrated the feasibility of using MR temperature maps to monitor treatment. After inducing lesions in the brain of trepanned monkeys with a 1.5-MHz therapeutic transducer (McDannold *et al.*, 2003), the same team performed MR-guided sonications in monkeys through an intact skull with a pre-clinical lower frequency transducer (670 kHz; Hynynen, 2006). With this 670-kHz transducer, it was not possible to induce brain tissue coagulation at the focus without overheating the brain surface because of the limited antenna gain between the skull surface and the focal spot. Nevertheless, the study provided valuable safety data: the intensity at the skull surface can be increased up to 3.0 W/cm^2 without damaging the brain surface.

In the present study, the use of a higher frequency sufficiently increased the antenna gain to induce lesion in the brain without damaging the brain surface. Such a high-frequency approach requires an accurate estimation of the aberrations induced by the skull of the animal and precise stereotactic positioning. A drawback of this approach is the 90-min simulation time required to calculate the complex shape of the ultrasonic signals that need to be emitted through the intact skull in a monkey.

B. Threshold for tissue damage

Previous ultrasonic brain tissue destruction experiments provided useful data for treatment dose planning. McDannold *et al.* (2003) reported accumulated treatment doses ranging from 129 to more than 240 Eq min at 43 °C. Histologically confirmed tissue damage was observed for each location, so that the threshold for tissue damage appeared to be less than 129 Eq. min at 43 °C. This is consistent with the thermal dose threshold for tissue damage evaluated in this study: between 90 and 280 Eq. min at 43 °C.

Cohen *et al.* (2007) correlated tissue damage to MR-measured peak temperature and total acoustic power. Energy requirements to achieve thermocoagulated lesions were between 75 and 100 W. In all targets that showed an effect, peak temperature at the focus was higher than 62 °C, whereas no effect was observed when the peak temperature was lower than 60 °C. Nevertheless, those data were not sufficient to evaluate the thermal dose. The peak temperature

TABLE I. Results.

Monkey no.	Necrosis	Thermal dose (Eq min 43 °C)	Side effect	Neurological score	Corticoids
1 Left hemisphere	No	26	None	Normal	No
1 Right hemisphere	Yes	803	Subcutaneous edema, petechia in the brain	Normal	No
2 Left hemisphere	Yes	288	None	Normal	No
2 Right hemisphere	Yes	26163	Edema in the brain, skin burn	Listless and ate less	No
3 Left hemisphere	No	89	None	Normal	Yes
3 Right hemisphere	No	19	None	Normal	Yes
4 Left hemisphere	Yes	2.6e8	None	Normal	Yes
4 Right hemisphere	No	2.5e7	Minor subcutaneous edema	Normal	Yes
5	NA	NA	Died during anesthesia (during CT scans)	Normal	No

itself might give an indication, but is not representative of the biological effects. Biological effects linearly depend on the time during which a given temperature is applied to a tissue.

Nevertheless, as sonication times (between 12 and 16 s) were comparable to the ones used in this study (10 s), a rough comparison between our investigation and that of Cohen *et al.* (2007) can be made. Consequently, we determined the peak temperature threshold corresponding to our thermal dose threshold: between 53 °C and 57 °C. This was comparable to the one obtained by Cohen *et al.* (2007).

C. Protection of skin and bone

In the past fifteen years, clinical devices have demonstrated the ability to safely ablate tumors located outside the skull. In the absence of air and bone structures in the ultrasonic pathway, no side effects have been reported. For prostate adenocarcinoma treatment, long-term follow-up data are now available (1–10 yr; Poissonnier *et al.*, 2007) and reveal that the prostate specific antigen levels remain low and the negative biopsy rate remains around 90%. Nevertheless, for liver adenocarcinoma treatments, skin burns have been reported (Wu *et al.*, 2004a; Wu *et al.*, 2004b; Kennedy *et al.*, 2004; Li *et al.*, 2007). Indeed, due to the high value of the absorption coefficient of the bone (Goss *et al.*, 1979), ribs overheating can be quite important even though the pressure level at the outer surface of the body is significantly lower than the pressure level at the targeted location. *In vivo* measurements of temperature elevation in pork ribs were reported by Daum *et al.* (1999) via MR temperature monitoring. Temperature increase during sonication was five times higher on the ribs than in the intercostal space. Such a potentially high absorption has to be taken into account for transcranial treatment. This is why an active cooling system was included in our system, with circulating water maintained at 15 °C. In all our experiments, the temperature of the skin during sonication was 20 °C, as recorded by the thermocouple. To avoid perturbing the focusing, the thermocouple was inserted at the edge of the beam, in between the scalp and the coupling membrane. The recorded temperature was set by the temperatures of the cooling bath and the animal head. It did not reflect the maximum temperature that was reached at the skin surface over the cross-section of the beam. The cooling time between sonications (20 s) was sufficient to avoid skin burns, confirming previous results obtained in sheep *in vivo* (Pernot *et al.*, 2007). There is a narrow safety window between thermal lesions at the focus only and thermal lesions accompanied by side effects. The small size of the available animal brain cavity (swine, sheep or monkey) exacerbates this narrow window. The skull is close to the target and its overheating is more likely to induce side effects than the skull in humans. Nevertheless, it highlights the need to optimize the acoustical parameters in order to deliver the minimum therapeutic dose to the focus.

D. MR monitoring

In the present study performed without MR, all the treatment planning was undertaken numerically and no particular monitoring was performed during treatment (except for rectal temperature measurement and the monitoring of the applied electrical power on one channel). Temperature increase at the focus and accumulated thermal doses were estimated using the bioheat equation, giving results that correlated well with those of previous clinical studies (McDannold *et al.*, 2003; Cohen *et al.*, 2007). No lesions could be seen during histological examination in one tissue sample despite a high thermal dose (far left point, at the bottom of Fig. 7). This indicates that the pressure at the focus was far below the expected one. This could have been due to acoustic cavitation in the water-coupling balloon. Such acoustic bubbles could have created an ultrasonic wall, preventing the ultrasound from entering the brain. Whatever the reason, a device should be added to the system to monitor the treatment. MR monitoring is the most suited solution for this application. An MR compatible version of this prototype has now been designed and constructed, where MR is used to guide non-invasive ultrasound brain therapy.

V. CONCLUSIONS

A non-invasive protocol for ultrasonic thermal ablation of brain tissues through the intact skull was proposed and validated in monkeys. Transcranial focusing was made possible by the prediction and correction of the defocusing effect of the skull, using a full 3D finite-difference simulation code together with stereotactic CT images. The thermal threshold for lesions was determined to be in the interval [90,280] Eq min at 43 °C. Our *in vivo* results are encouraging and an MR compatible version of this prototype is under development for clinical transfer with MR guidance and monitoring. The treatment of neurological disorders (like essential tremors) and recurrent deep-seated metastases is certainly one of the best indications of this method. Moreover, the treatment of other tumors with well-defined borders could also be feasible (meningiomas, schwannomas). Moreover, the possibility to selectively open the blood brain barrier with ultrasound to enhance local drug delivery could create new avenues of treating various brain disorders.

ACKNOWLEDGMENTS

This work was funded by the Fondation de l'Avenir, supporting the cost of the animals' preparation and handling. The authors wish to thank the IMM Research group (www.imm-recherche.com) for their support.

Andrews, D. W., Bednarz, G., Evans, J. J., and Downes, B. (**2006**). "A review of 3 current radiosurgery systems," Surg. Neurol. **6**, 559–564.

Aubry, J.-F., Tanter, M., Pernot, M., Thomas, J.-L., and Fink, M. (**2003**). "Experimental demonstration of non invasive transskull adaptive focusing based on prior CT scans," J. Acoust. Soc. Am. **113**, 85–93.

Chang, S. D., and Adler, J. R. (**2001**). "Current status and optimal use of radiosurgery," Oncology-New York **2**, 209–216.

Chilowsky, C., and Langevin, P. (**1916**). Procédés et appareils pour la production de signaux sous-marins dirigés et pour la localisation à distance d'obstacles sous-marins. French patent no 502913.

Cohen, Z. R., Zaubermann, J., Harnof, S., Mardor, Y., Nass, D., Zadicario, E., Hananel, A., Castel, D., Faibel, M., and Ram, Z. (**2007**). "Magnetic resonance imaging-guided focused ultrasound for thermal ablation in the brain: A feasibility study in a swine model," Neurosurgery **4**, 593–600.

Daum, D. R., Smith, N. B., King, R., and Hynynen, K. (**1999**). "In vivo demonstration of noninvasive thermal surgery of the liver and kidney using an ultrasonic phased array," Ultrasound Med. Biol. **25**, 1087–1098.
Fry, F. J., and Goss, S. A. (**1980**). "Further studies of the transkull transmission of an intense focused ultrasonic beam: Lesion production at 500 kHz," Ultrasound Med. Biol. **6**(1), 33–38.
Fry, F. J., Kossoff, G., Eggleton, R. C., and Dunn, F. (**1970**). "Threshold ultrasonic dosages for structural changes in the mammalian brain," J. Acoust. Soc. Am. **48**, 1413–1417.
Fry, W. J. (**1956**). "Ultrasound in neurology," Neurology **6**, 693–704.
Fry, W. J., Barnar, J. W., Fry, F. J., Krumins, R. F., and Brennan, J. F. (**1955**). "Ultrasonic lesions in the mammalian central nervous system," Science **122**, 517–518.
Fry, W. J., Mosberg, W. H., Barnard, J. W., and Fry, F. J. (**1954**). "Production of focal destructive lesions in the central nervous system with ultrasound," J. Neurosurg. **11**, 471–478.
Goss, S. A., Frizzell, L. A., and Dunn, F. (**1979**). "Ultrasonic absorption and attenuation in mammalian tissues," Ultrasound Med. Biol. **5**, 181–186.
Harvey, E. N., and Loomis, A. L. (**1928**). "High frequency sound waves of small intensity and their biological effects," Nature **121**, 622–624.
Hynynen, K., and Jolesz, F. A. (**1998**). "Demonstration of potential noninvasive ultrasound brain therapy through an intact skull," Ultrasound Med. Biol. **24**, 275–283.
Hynynen, K., McDannold, N., Clement, G., Jolesz, F., Zadicario, E., Killiany, R., Moore, T., and Rosen D. (**2006**). "Pre-clinical testing of a phased array ultrasound system for MRI-guided noninvasive surgery of the brain-A primate study," Eur. J. Radiol. **59**(2), 149–156.
Jeanmonod, D., Werner, B., Morel, A., Michels, L., Zadicario, E., Schiff, G., and Martin, E. (**2012**). "Transcranial magnetic resonance imaging–guided focused ultrasound: noninvasive central lateral thalamotomy for chronic neuropathic pain," Neurosurg. Focus **32**, E1.
Jolesz, F. (**2008**). "MRI-guided thermal ablations of brain tumors – clinical experience, oral communication," *MRgFUS Symposium*, Washington.
Kennedy, J. E., Wu, F., ter Haar, G. R., Gleeson, F. V., Phillips, R. R., Middleton, M. R., and Cranston, D. (**2004**). "High-intensity focused ultrasound for the treatment of liver tumors," Ultrasonics **42**, 931–935.
Li, J. J., Xu, G. L., and Gu, M. F. (**2007**). "Complications of high intensity focused ultrasound in patients with recurrent and metastatic abdominal tumors," World J. Gastroenterol. **13**, 2747–2751.
Lindstrom, P. A. (**1954**). "Prefrontal ultrasonic irradiation-a substitute for lobotomy," AMA Arch. Neurol. Psychiatry **72**, 399–425.
Lynn, J. G., Zwemer, R. L., and Chick, A. J. (**1942**). "Biological application of focused ultrasonic waves," Science **96**, 119–120.
Marquet, F., Pernot, M., Aubry, J.-F., Montaldo, G., Marsac, L., Tanter, M., and Fink, M. (**2009**). "Non-invasive transcranial ultrasound therapy guided by 3D CT-scans: protocol validation and in-vitro results," Phys. Med. Biol. **54**, 2597–2613.
Martin, E., Jeanmonod, D., Morel, A., Zadicario, E., and Werner, B. (**2009**). "High-intensity focused ultrasound for noninvasive functional neurosurgery," Ann. Neurol. **66**, 858–861.
McDannold, N., Clement, G. T., Black, P., Jolesz, F., and Hynynen, K. (**2010**). "Transcranial magnetic resonance imaging- guided focused ultrasound surgery of brain tumors: initial findings in 3 patients," Neurosurgery **66**, 323–332.
McDannold, N., Moss, M., Killiany, R., Rosene, D. L., King, R. L., Jolesz, F. A., and Hynynen, K. (**2003**). "MRI-guided focused ultrasound surgery in the brain: tests in a primate model," Magn. Reson. Med. **49**, 1188–1191.
Monteith, S. J., Harnof, S., Medel, R., Popp, B., Wintermark, M., Lopes, M. B., Kassell, N. F., Elias, W. J., Snell, J., Eames, M., Zadicario, E., Moldovan, K., and Sheehan, J. (**2013a**). "Minimally invasive treatment of intracerebral hemorrhage with magnetic resonance-guided focused ultrasound," J. Neurosurg. **118**(5), 1035–1045.
Monteith, S., Sheehan, J., Medel, R., Wintermark, W., Eames, M., Snell, J., Kassell, N. F., and Elias, W. J. (**2013b**). "Potential intracranial applications of magnetic resonance–guided focused ultrasound surgery," J. Neurosurg. **118**, 215–221.
Pennes, H. H. (**1948**). "Analysis of tissue and arterial blood temperature in the resting human forearm," J. Appl. Physiol. **1**, 93–122.
Pernot, M., Aubry, J.-F., Tanter, M., Boch, A.-L., Marquet, F., Kujas, M., Seilhean, D., and Fink, M. (**2007**). "In vivo transcranial brain surgery with an ultrasonic time reversal mirror," J. Neurosurg. **106**, 1061–1066.
Pinton, G., Aubry, J.-F., and Tanter, M. (**2012**). "Direct phase projection and transcranial focusing of ultrasound for brain therapy," IEEE Trans. Ultrason. Ferroelectr. Freq. Control **59**, 1149–1159.
Poissonnier, L., Chapelon, J. Y., and Rouviere, O. (**2007**). "Control of prostate cancer by transrectal HIFU in 227 patients," Eur. Urol. **51**, 381–387.
Pulkkinen, A., Huang, Y., Song, J., and Hynynen, K. (**2011**). "Simulations and measurements of transcranial low-frequency ultrasound therapy: skull-base heating and effective area of treatment," Phys. Med. Biol. **56**(15): 4661–4683.
Sapareto, S. A., and Dewey, W. C. (**1984**). "Thermal dose determination in cancer therapy," Int. J. Radiat. Oncol. Biol. Phys. **10**, 787–800.
Sun, J., and Hynynen, K. (**1998**). "Focusing of therapeutic ultrasound through a human skull: a numerical study," J. Acoust. Soc. Am. **104**, 1705–1715.
Tanter, M., Pernot, M., Aubry, J. F., Montaldo, G., Marquet, F., and Fink, M. (**2007**). "Compensating for bone interfaces and respiratory motion in high intensity focused ultrasound," Int. J. Hyperthermia **23**, 141–151.
Thomas, J.-L., and Fink, M. (**1996**). "Ultrasonic beam focusing through tissue inhomogeneities with a time reversal mirror: Application to transskull therapy," IEEE Trans. Ultrason. Ferroelectr. Freq. Control **43**, 1122–1129.
Wood, R. W., and Loomis, A. L. (**1927**). "Physical and biological effects of high frequency sound of great intensity," Philos. Mag. **4**, 417–436.
Wu, F., Wang, Z. B., and Chen, W. Z. (**2004a**). "Extracorporeal high intensity focused ultrasound ablation in the treatment of 1038 patients with solid carcinomas in China: an overview," Ultrason. Sonochem. **11**, 149–154.
Wu, F., Zhi-Biao, W., Wen-Zhi, C., Hui, Z., Jin, B., Jian-Zhong, Z., Ke-Quan, L., Cheng-Bing, J., Fang-Lin, X., and Hai-Bing, S. (**2004b**). "Extracorporeal high intensity focused ultrasound ablation in the treatment of patients with large hepatocellular carcinoma," Ann. Surg. Oncol. **11**, 1061–1069.